Phase equilibria of Lennard-Jones dipolar plus quadrupolar fluids by Gibbs-ensemble Monte Carlo simulation

Girija S. Dubey* and Seamus F. O'Shea
Department of Chemistry, University of Lethbridge, Lethbridge, Alberta, Canada T1K 3M4
(Received 18 June 1993)

Gibbs simulation techniques have been used to calculate vapor-liquid equilibria of monatomic molecules having both dipoles and linear quadrupoles embedded in their Lennard-Jones cores. Results presented here include the coexistence curves and the estimates of the critical temperatures and densities for a range of values of both Q^{*2} and μ^{*2}, where $\mu^{*2}=\mu^2/(\epsilon\sigma^3)=1.00$ or 2.00 and $Q^{*2}=Q^2/(\epsilon\sigma^5)=1.00$, 1.50, 2.00, or 2.50. Our simulation results indicate that both T_c^* and ρ_c^* increase with increasing values of the electrostatic moments, and both are more sensitive to Q^{*2} than μ^{*2}.

PACS number(s): 64.70.Fx, 64.10.+h

I. INTRODUCTION

Vapor-liquid equilibria of fluids are of interest for many reasons. For example, one would like to understand the effect of different molecular parameters on the saturation properties. A phase diagram summarizes the behavior over a range of temperature and pressure, permits interpolation between measured data, and facilitates the determination of optimum conditions for specific applications. Since vapor-liquid equilibria are sensitive to intermolecular potentials, the relationship may be studied from both points of view. Furthermore, phase equilibria for models can provide insight into the nature of this sensitivity, and observed equilibria may be used cautiously to investigate potentials.

The problem of obtaining phase diagrams from model potential via computer simulation has been a challenge ever since the first simulation studies [1] were reported. A major advance in the use of molecular simulations in the study of vapor-liquid equilibria has been the use of the Gibbs-ensemble [2–4] method. This permits the direct simulation of bulk vapor and liquid phases satisfying the conditions of phase equilibrium. Gibbs-ensemble Monte Carlo simulations have now been performed for a number of potential models, including pure Lennard-Jones fluids and mixtures [5,6], Stockmayer fluids and their mixtures, square-well fluids, and polyatomic fluids and mixtures [7-10], the symmetrical nonadditive hard-sphere system [11], the hard-core two-Yukawa fluid [12], the Lennard-Jones fluids with a quadrupole interaction [13,14], hard-core Yukawa fluids [15], the nonspherical Gay-Berne fluid [16], square-well diatomics [17], more realistic models for alkanes and water [18,19], and hard ellipsoids [20].

The purpose of this paper is to apply the Gibbs-ensemble method to a generalized Stockmayer fluid consisting of Lennard-Jones (LJ) spheres with embedded point dipoles and linear quadrupoles. Our calculations provide accurate vapor-liquid coexistence data for these fluids. There are several reasons why model fluids of this type are of interest. The combined effects due to dipoles and quadrupoles have potential implications for the theory of polar solutions. One advantage is that these models are still sufficiently simple for theoretical methods to be applied. Although dipoles are recognized as being crucial for a realistic modeling of dielectric behavior, molecular quadrupoles are expected to play a significant role through their impact on the mutual orientation of the molecules.

To the best of our knowledge, the calculated coexistence data presented here constitute the only available simulation information on vapor-liquid equilibria of monatomic molecules having both dipoles and linear quadrupoles embedded in their Lennard-Jones cores. We are also interested in studying the changes in the phase diagram as a function of the molecular electrostatic moments. Since finite-size effects in the Gibbs ensemble are reported to be smaller than in other ensembles [21], we believe that our estimates of the critical properties of fluids are reliable. Our simulation data now make it possible to assess the validity of other theories, e.g., those in the form of the Padé approximants [22,23] based on perturbation theory, the linearized hypernetted chain (LHNC), or generalized-mean-field (GMF) theory [24].

The rest of the paper is organized as follows. The model potentials and computational details of our simulations are presented in Sec. II. Section III contains the results of the Gibbs-ensemble simulations for the phase equilibria as well as the critical behavior of our simulation results. We also present a critical comparison between the behavior of our results and those of Stockmayer and quadrupolar LJ fluids. Section IV is devoted to a summary and the conclusions of our results.

II. MODEL POTENTIALS AND COMPUTATIONAL DETAILS

The intermolecular potential models we used in our calculations have the general form

*Present address: New York University, New York, NY 10003.

$$U(\hat{\mathbf{r}},\omega_1,\omega_2)=U(12)=U^0(12)+U^{\mu\mu}(12)+U^{\mu q}(12)+U^{QQ}(12)\ .$$

Here $\hat{\mathbf{r}}$ is the vector joining the centers of mass of the molecules, $\omega_i=(\theta_i,\phi_i)$ is the orientation of molecule i, and U^0 is the isotropic part of the potential which, in this study is the Lennard-Jones 12-6 potential. $U^{\mu\mu}$, $U^{\mu q}$, and U^{QQ} are the contributions due to dipole-dipole, dipole-quadrupole, and quadrupole-quadrupole interactions, respectively:

$$U^{LJ}(r)=4\epsilon[(\sigma/r)^{12}-(\sigma/r)^6]\ , \tag{1}$$

$$U_{ij}^{\mu\mu}=(\mu^{*2}/r_{ij}^3)[\cos\gamma_{ij}-3\cos\theta_i\cos\theta_j]\ , \tag{2}$$

$$U_{ij}^{\mu Q}=(3\mu^*Q^*/2r_{ij}^4)\times[(\cos\theta_i-\cos\theta_j)\times(1+5\cos\theta_i\cos\theta_j-2\cos\gamma_{ij})]\ , \tag{3}$$

$$U_{ij}^{QQ}=(3Q^{*2}/4r_{ij}^5)\times[1-5\cos^2\theta_i-5\cos^2\theta_j-15\cos^2\theta_i\cos^2\theta_j+2(\cos\gamma_{ij}-5\cos\theta_i\cos\theta_j)^2]\ , \tag{4}$$

where Q_i^* and μ_i^*, respectively, are the dipole and quadrupole moments on molecule i, r_{ij} is the distance between molecules i and j, and

$$\cos\theta_i=\hat{\mathbf{e}}_i\cdot\hat{\mathbf{r}}_{ij},\quad \cos\theta_j=\hat{\mathbf{e}}_j\cdot\hat{\mathbf{r}}_{ij},\quad \gamma_{ij}=\hat{\mathbf{e}}_i\cdot\hat{\mathbf{e}}_j\ . \tag{5}$$

$\hat{\mathbf{r}}_{ij}$ is a unit vector pointing from molecule i to molecule j, and $\hat{\mathbf{e}}_i$ and $\hat{\mathbf{e}}_j$ are unit vectors along the molecular axes.

Our implementation of the Gibbs ensemble is essentially the same as that described by Panagiotopoulos and coworkers [2,5], and the reader is referred to these references for a more detailed description of the technique. Our calculations were performed mostly with $N=500$ particles. For the $N=500$ particles system we initialized the simulation with 350 particles at a liquidlike density in one box, and 150 particles at a lower, vaporlike density for the other box. Generally the simulations were started either with the particles of each box on the sites of a face-centered-cubic (fcc) lattice, or in an equilibrated state from a lower temperature. A simulation cycle in the Gibbs-ensemble Monte Carlo method comprises three distinct types of moves: individual molecule displacements, interbox volume displacements, and interbox particle transfers. The relative numbers of each type of move are chosen to optimize convergence. In these calculations, for each cycle we used a single attempted displacement of each molecule, followed by one trial volume move, and a number of attempted particle transfers. In the individual molecule displacements, the particles are chosen and displaced randomly, both translationally and orientationally, within the boxes, following the well established Metropolis scheme for canonical NVT simulations [25]. Particle transfers were achieved by creating a particle at a random position in one subsystem and annihilating a randomly chosen particle in the other subsystem. The number of attempted particle transfers was adjusted to achieve a success rate of between $\sim 1-3\,\%$. The calculation required for the insertion step permitted the evaluation of the chemical potential by Widom's method [26].

The Lennard-Jones potential was truncated at half the box size, and the usual long tail corrections were applied to energy and pressure. The simulation of phase equilibrium for a given state point involved a total of $N_{\text{cycle}}=8000$ cycles. After equilibrating the system for 2000 cycles; 10^6 attempted single-particle displacements, a further 6000 cycles were performed to accumulate the averages for the properties of the two coexisting phases. By repeating the simulations for a series of temperatures, the vapor-liquid coexistence curves were determined.

The algorithm used in this paper was tested in a number of special cases. When both the dipole and quadrupole moments are zero, the results for the pure LJ system were reproduced [2,14]. Furthermore, when the quadrupole moment is zero, we obtain the results for the Stockmayer fluid [6]. Finally, when the dipole moment is zero our results are the same as the quadrupolar LJ fluid of Smit and Williams [14] and Stapleton *et al.* [13]. These results for limiting cases give us added confidence that the details of the algorithm are correct, and the calculations are long enough to ensure that our data are representative of the thermodynamics conditions.

The long-range dipolar interactions were handled by means of the minimum image convention, rather than by the Ewald-Kornfeld summation technique [27]. For the Stockmayer fluid, using $N=500$ particles without the Ewald summation, our results match those of Smit *et al.* [6] (see Table I) and unpublished work from this laboratory using the Ewald-Kornfeld summation for the dipole-dipole interaction.

III. NUMERICAL RESULTS AND DISCUSSION

The phase equilibrium results from our Gibbs-ensemble Monte Carlo simulations are presented in Tables II–VII. The results for various values of μ^{*2} and Q^{*2} are tabulated in reduced units defined as $T^*=kT/\epsilon$, $E^*=E/N\epsilon$, $\rho^*=\rho\sigma^3$, and $P^*=P\sigma^3/\epsilon$. The resulting vapor-liquid coexistence curves are shown in Figs. 1–6. The values of the critical constants are given in Table VIII. All the averages shown in Tables II–VII were obtained over periods of 6000 cycles.

The uncertainty reported with each result is the standard deviation of averages calculated over 100-cycle blocks during the production phase of simulation. In some cases simulations were repeated starting from different initial conditions, including different overall density, or with a different number attempted molecules transfer per cycle. We found that the results obtained were the same within their combined uncertainties. These are consistent with equivalent results of other investigators (e.g., compare Tables I and II). Nevertheless these uncertainties must be treated with some care since, at best, they represent a "local" estimate of the variability; the coexistence curves show roughness which is somewhat larger than the uncertainties but which is unlikely to be physically correct.

Metropolis Monte Carlo simulations for a canonical

TABLE I: Comparison of results using the minimum image (MI) convention in the Gibbs ensemble for a Stockmayer fluid with those of Smit *et al.* using Ewald-Kornfeld (EK) [6] for various dipolar strengths. N is the total number of particles, T^* is the reduced temperature, ρ_x^* is the reduced density, P_x^* $(=P_x\sigma^3/\epsilon)$ is the reduced pressure, E_x^* $[=E_x/(N\epsilon)]$ is the reduced energy, and μ_x^* $[=\mu_x/(N\epsilon)]$ is the reduced chemical potential in the x phase.

			Vapor phase				Liquid phase			
N	T^*	Method	ρ_v^*	P_v^*	E_v^*	μ_v^*	ρ_l^*	P_l^*	E_l^*	μ_l^*
					$\mu^{*2}=1.0$					
512	1.00	EK	0.0150 ±0.002	0.0140 ±0.002	−0.1800 ±0.050	−4.3700	0.7550 ±0.005	0.0100 ±0.030	−6.1600 ±0.050	−4.4400
500	1.00	MI	0.0140	0.0134	−0.1790	−4.4545	0.7561	0.0220	−6.1519	−4.3416
512	1.10	EK	0.0270 ±0.007	0.0250 ±0.003	−0.3200 ±0.070	−4.3200	0.6970 ±0.009	0.0100 ±0.020	−5.6000 ±0.070	−4.2800
500	1.10	MI	0.0284	0.0274	−0.3350	−4.2608	0.7017	0.0392	−5.6369	−4.0872
216	1.30	EK	0.0800 ±0.010	0.0700 ±0.010	−0.8000 ±0.1	−4.0700	0.5700 ±0.020	0.0700 ±0.030	−4.500 ±0.1	−4.0800
500	1.30	MI	0.1031	0.0865	−1.0361	−3.9518	0.5783	0.0883	−4.5463	−3.9221
					$\mu^{*2}=2.0$					
512	1.15	EK	0.0120 ±0.002	0.0120 ±0.002	−0.2300 ±0.090	−5.2900	0.7590 ±0.007	0.0000 ±0.05	−7.5600 ±0.060	−5.1100
500	1.15	MI	0.0118	0.0132	−0.2576	−5.3269	0.7601	0.0010	−7.6037	−5.3177
216	1.30	EK	0.0400 ±0.010	0.0340 ±0.004	−0.6100 ±0.100	−4.8700	0.6900 ±0.010	0.0200 ±0.040	−6.7000 ±0.200	−5.1400
500	1.30	MI	0.0341	0.0374	−0.6392	−4.9374	0.6886	0.360	−6.7821	−5.0061
216	1.40	EK	0.0600 ±0.010	0.0580 ±0.008	−0.9000 ±0.30	−4.8500	0.6300 ±0.020	0.0300 ±0.060	−6.2000 ±0.2	−4.8700
500	1.40	MI	0.0575	0.0589	−0.9597	−4.8067	0.6342	0.0516	−6.1828	−4.8207

TABLE II. Summary of the results of the Monte Carlo simulation in the Gibbs ensemble for a dipolar plus quadrupolar Lennard-Jones fluid for various dipolar and quadrupolar strengths. N is the total number of particles, T^* is the reduced temperature, N_{cycle} is the number of Monte Carlo cycles, ρ_x^* is the reduced density, P_x^* $(=P_x\sigma^3/\epsilon)$ is the reduced pressure, E_x^* $[=E_x/(N\epsilon)]$ is the reduced energy, μ_x^* $[=\mu_x/(N\epsilon)]$ is the reduced chemical potential in the x phase, and ρ^* is overall simulation density of each temperature run.

$Q^{*2}=1.00$				Vapor phase					Liquid phase			
N	T^*	N_{cycle}	ρ^*	ρ_v^*	P_v^*	E_v^*	μ_v^*	ρ_l^*	P_l^*	E_l^*	μ_l^*
						$\mu^{*2}=1.00$					
500	1.4	8000	0.063	0.022 ±0.002	0.027 ±0.001	−0.479 ±0.010	−5.722 ±0.20	0.783 ±0.004	0.035 ±0.001	−8.880 ±0.038	−5.618 ±0.35
500	1.45	8000	0.063	0.031 ±0.003	0.038 ±0.002	−0.639 ±0.005	−5.547 ±0.10	0.760 ±0.004	0.048 ±0.002	−8.535 ±0.056	−5.278 ±0.40
500	1.50	8000	0.063	0.039 ±0.003	0.046 ±0.004	−0.748 ±0.004	−5.500 ±0.10	0.732 ±0.003	0.062 ±0.007	−8.169 ±0.0172	−5.308 ±0.30
500	1.55	8000	0.063	0.048 ±0.004	0.057 ±0.006	−0.861 ±0.001	−5.423 ±0.10	0.698 ±0.006	0.068 ±0.002	−7.769 ±0.029	−5.569 ±0.10
500	1.60	8000	0.140	0.073 ±0.003	0.083 ±0.006	−1.260 ±0.05	−5.207 ±0.10	0.679 ±0.006	0.097 ±0.008	−7.463 ±0.06	−5.221 ±0.10
500	1.65	8000	0.140	0.094 ±0.003	0.100 ±0.004	−1.522 ±0.048	−5.133 ±0.10	0.631 ±0.002	0.104 ±0.007	−6.919 ±0.04	−5.161 ±0.10
500	1.70	8000	0.140	0.099 ±0.004	0.110 ±0.004	−1.540 ±0.050	−5.168 ±0.10	0.587 ±0.011	0.116 ±0.001	−6.457 ±0.09	−5.030 ±0.20
500	1.75	8000	0.265	0.149 ±0.005	0.141 ±0.002	−2.151 ±0.050	−5.010 ±0.10	0.533 ±0.018	0.163 ±0.013	−5.893 ±0.009	−4.932 ±0.20

TABLE III. Vapor-liquid coexistence data from the Gibbs-ensemble Monte Carlo simulation for $\mu^{*2}=1.00$ and $Q^{*2}=1.50$. See Table II for details.

$Q^{*2}=1.50$			Vapor phase					Liquid phase			
N	T^*	N_{cycle}	ρ^*	ρ_v^*	P_v^*	E_v^*	μ_v^*	ρ_l^*	P_l^*	E_l^*	μ_l^*
						$\mu^{*2}=1.00$					
500	1.70	8000	0.063	0.025	0.037	−0.72	−6.79	0.80	0.041	−10.94	−6.533
				±0.004	±0.001	±0.018	±0.10	±0.006	±0.006	±0.083	±0.30
500	1.80	8000	0.063	0.037	0.054	−0.961	−6.613	0.718	0.064	−9.730	−6.688
				±0.003	±0.003	±0.023	±0.10	±0.010	±0.004	±0.172	±0.10
500	1.90	8000	0.122	0.069	0.094	−1.567	−6.208	0.660	0.087	−8.802	−6.040
				±0.001	±0.005	±0.049	±0.10	±0.007	±0.008	±0.120	±0.20
500	2.00	8000	0.187	0.108	0.135	−2.125	−6.040	0.599	0.137	−7.962	−5.895
				±0.002	±0.004	±0.035	±0.15	±0.017	±0.001	±0.192	±0.36
500	2.05	8000	0.254	0.164	0.171	−2.988	−5.861	0.545	0.179	−7.314	−5.880
				±0.012	±0.003	±0.16	±0.09	±0.012	±0.002	±0.15	±0.07

TABLE IV. Vapor-liquid coexistence data from the Gibbs-ensemble Monte Carlo simulation for $\mu^{*2}=1.00$ and $Q^{*2}=2.00$. See Table II for details.

$Q^{*2}=2.00$			Vapor phase					Liquid phase			
N	T^*	N_{cycle}	ρ^*	ρ_v^*	P_v^*	E_v^*	μ_v^*	ρ_l^*	P_l^*	E_l^*	μ_l^*
						$\mu^{*2}=1.00$					
500	2.00	8000	0.122	0.032	0.049	−1.419	−7.708	0.824	0.047	−13.285	−7.924
				±0.002	±0.006	±0.012	±0.20	±0.006	±0.002	±0.059	±0.10
500	2.10	8000	0.122	0.037	0.063	−1.266	−7.777	0.753	0.050	−12.099	−7.738
				±0.002	±0.004	±0.026	±0.10	±0.017	±0.008	±0.212	±0.10
500	2.20	8000	0.119	0.067	0.102	−1.993	−7.288	0.713	0.119	−11.315	−7.374
				±0.002	±0.009	±0.034	±0.13	±0.001	±0.002	±0.230	±0.15
500	2.30	8000	0.183	0.096	0.141	−2.535	−7.145	0.607	0.154	−09.772	−7.366
				±0.003	±0.002	±0.046	±0.38	±0.011	±0.008	±0.171	±0.10
500	2.35	8000	0.233	0.124	0.173	−3.066	−6.980	0.578	0.189	−9.380	−6.763
				±0.011	±0.009	±0.25	±0.10	±0.015	±0.003	±0.123	±0.40

TABLE V. Vapor-liquid coexistence data from the Gibbs-ensemble Monte Carlo simulation for $\mu^{*2}=1.00$ and $Q^{*2}=2.50$. See Table II for details.

$Q^{*2}=2.50$			Vapor phase					Liquid phase			
N	T^*	N_{cycle}	ρ^*	ρ_v^*	P_v^*	E_v^*	μ_v^*	ρ_l^*	P_l^*	E_l^*	μ_l^*
						$\mu^{*2}=1.00$					
500	2.40	8000	0.172	0.046	0.081	−2.215	−8.701	0.823	0.058	−15.413	−8.281
				±0.001	±0.002	±0.009	±0.10	±0.007	±0.009	±0.032	±0.60
500	2.50	8000	0.169	0.066	0.111	−2.604	−8.467	0.791	0.140	−14.659	−8.265
				±0.005	±0.007	±0.013	±0.10	±0.014	±0.005	±0.110	±0.30
500	2.60	8000	0.169	0.080	0.139	−2.855	−8.459	0.697	0.153	−13.079	−8.720
				±0.001	±0.008	±0.018	±0.20	±0.007	±0.001	±0.104	±0.09
500	2.70	8000	0.250	0.119	0.191	−3.807	−8.154	0.616	0.201	−11.738	−8.305
				±0.001	±0.006	±0.021	±0.20	±0.011	±0.002	±0.145	±0.10
500	2.75	8000	0.261	0.153	0.222	−4.337	−8.040	0.563	0.229	−10.825	−8.068
				±0.012	±0.003	±0.031	±0.10	±0.014	±0.002	±0.167	±0.10

TABLE VI. Vapor-liquid coexistence data from the Gibbs-ensemble Monte Carlo simulation for $\mu^{*2}=2.00$ and $Q^{*2}=1.00$. See Table II for details.

$Q^{*2}=1.00$			Vapor phase					Liquid phase			
N	T^*	N_{cycle}	ρ^*	ρ_v^*	P_v^*	E_v^*	μ_v^*	ρ_l^*	P_l^*	E_l^*	μ_l^*
						$\mu^{*2}=2.00$					
500	1.60	8000	0.270	0.026	0.035	−0.828	−6.434	0.781	0.033	−10.190	−6.769
				±0.001	±0.002	±0.040	±0.30	±0.002	±0.003	±0.014	±0.09
500	1.65	8000	0.270	0.031	0.043	−0.879	−6.391	0.746	0.035	−9.681	−6.735
				±0.004	±0.003	±0.063	±0.40	±0.006	±0.008	±0.062	±0.08
500	1.70	8000	0.270	0.041	0.054	−1.090	−6.255	0.717	0.053	−9.298	−6.193
				±0.002	±0.004	±0.069	±0.10	±0.006	±0.007	±0.043	±0.10
500	1.75	8000	0.269	0.043	0.057	−1.101	−6.374	0.682	0.050	−8.843	−6.403
				±0.001	±0.003	±0.079	±0.15	±0.008	±0.004	±0.051	±0.10
500	1.80	8000	0.269	0.061	0.081	−1.458	−6.177	0.651	0.099	−8.417	−5.976
				±0.004	±0.003	±0.02	±0.13	±0.005	±0.001	±0.058	±0.26
500	1.85	8000	0.269	0.084	0.099	−1.859	−5.995	0.636	0.112	−8.135	−6.183
				±0.002	±0.009	±0.057	±0.2	±0.004	±0.003	±0.032	±0.05
500	1.90	8000	0.269	0.121	0.126	−2.487	−5.849	0.591	0.138	−7.608	−5.881
				±0.002	±0.004	±0.050	±0.10	±0.011	±0.001	±0.091	±0.10
500	1.95	8000	0.269	0.134	0.142	−2.605	−5.861	0.516	0.132	−6.825	−5.720
				±0.005	±0.002	±0.050	±0.06	±0.018	±0.001	±0.01	±0.12

ensemble are believed to overestimate the critical temperature [8]. To obtain precise estimates of the critical properties of the fluids, we have used these vapor-liquid equilibrium data to estimate the critical temperatures and densities. For this purpose, we have fitted our results to the law of rectilinear diameters [28] and a power law near the critical point:

$$(\rho_l^*+\rho_v^*)/2=A(T^*-T_c^*)+B\ , \tag{6}$$

$$\rho_l^*-\rho_v^*=C\left|1-\frac{T^*}{T_c^*}\right|^{\beta}, \tag{7}$$

where ρ_v^* and ρ_l^* are the saturation vapor and liquid densities at temperature T^*. In the above relations A, B, and C are constants to be determined from the data, and β is a known constant, the critical exponent ($\beta=0.32$ [28]). Equation (7) can be linearized by taking the βth root, and by fitting the simulation coexistence densities at different temperatures for every value of μ^{*2} and Q^{*2} included in Tables II and VII, T_c^* can be determined. Using the value T_c^* for every value of μ^{*2} and Q^{*2}, again fitting the simulation coexistence densities in Eq. (6), we obtain the value of ρ_c^*. The values of critical constants are presented in the Table VIII.

Because we are using 500 particles, increasing the system size should have a negligible effect on the Gibbs simulations reported here, and the critical parameters given in Table VIII should be close to those of the corresponding infinite system. There are no theoretical results available in the literature for comparison with ours.

Overall, the results suggest that the critical tempera-

TABLE VII. Vapor-liquid coexistence data from the Gibbs-ensemble Monte Carlo simulation for $\mu^{*2}=2.00$ and $Q^{*2}=2.00$. See Table II for details.

$Q^{*2}=2.00$			Vapor phase					Liquid phase			
N	T^*	N_{cycle}	ρ^*	ρ_v^*	P_v^*	E_v^*	μ_v^*	ρ_l^*	P_l^*	E_l^*	μ_l^*
						$\mu^{*2}=2.00$					
500	2.20	8000	0.122	0.029	0.051	−1.477	−8.863	0.813	0.048	−14.657	−8.306
				±0.009	±0.001	±0.040	±0.10	±0.003	±0.004	±0.029	±0.60
500	2.30	8000	0.122	0.046	0.077	−2.134	−8.454	0.764	0.075	−13.679	−8.798
				±0.001	±0.002	±0.063	±0.40	±0.006	±0.002	±0.081	±0.60
500	2.40	8000	0.122	0.067	0.106	−2.739	−8.183	0.713	0.109	−12.811	−8.029
				±0.001	±0.003	±0.069	±0.10	±0.004	±0.009	±0.043	±0.24
500	2.50	8000	0.183	0.090	0.140	−3.125	−8.155	0.657	0.146	−11.824	−8.505
				±0.003	±0.002	±0.079	±0.45	±0.007	±0.004	±0.082	±0.10
500	2.55	8000	0.228	0.114	0.161	−3.808	−7.850	0.564	0.141	−10.645	−7.920
				±0.003	±0.003	±0.02	±0.20	±0.005	±0.008	±0.07	±0.10
500	2.60	8000	0.228	0.151	0.200	−4.431	−7.806	0.550	0.230	−10.246	−7.391
				±0.004	±0.009	±0.057	±0.10	±0.003	±0.003	±0.04	±0.56

TABLE VIII. Estimates of the critical temperature T_c^* and critical density ρ_c^* for various dipolar strengths μ^{*2} and quadrupolar strengths Q^{*2}.

μ^{*2}	Q^{*2}	T_c^*	ρ_c^*
1.00	1.00	1.79 ±0.02	0.33 ±0.01
1.00	1.50	2.09 ±0.02	0.34 ±0.01
1.00	2.00	2.42 ±0.02	0.33 ±0.01
1.00	2.50	2.80 ±0.03	0.35 ±0.01
2.00	1.00	2.00 ±0.02	0.32 ±0.01
2.00	2.00	2.65 ±0.03	0.33 ±0.01

ture is sensitive to variation in Q^{*2} while μ^{*2} is fixed (see Fig. 7). The critical temperature increases with Q^{*2} at fixed μ^{*2}, and it also increases with μ^{*2} at fixed Q^{*2}, but less strongly. The critical volume, on the other hand, is insensitive to μ^{*2} at fixed Q^{*2}, but may increase slightly with Q^{*2} at fixed μ^{*2}. The volume effect is probably near the limit of our ability to measure it reliably, and may be an artifact. However, an argument in favor of such a result is easy to find: dipolar interactions supply relatively little binding energy to dense fluids because of the well-known difficulty of packing dipoles in three dimensions; whereas quadrupole interactions, although intrinsically weaker, contribute relatively more to the packing energies by virtue of their geometrical properties. Critical constants are available in the literature for Stockmayer

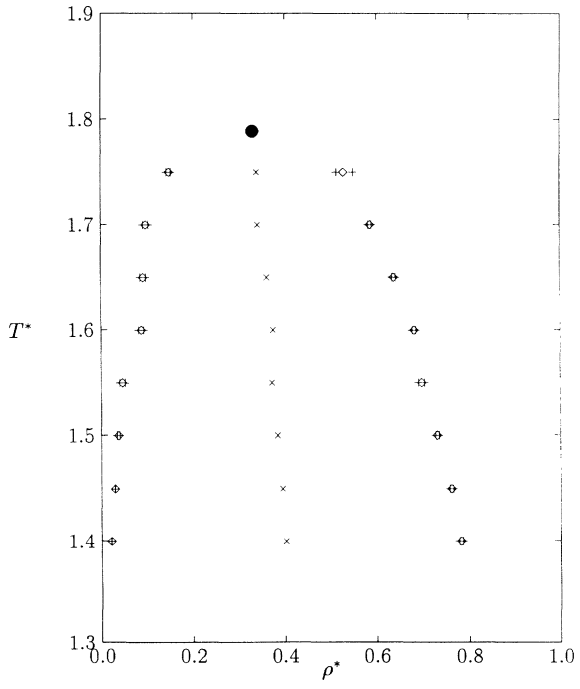

FIG. 1. Vapor-liquid coexistence curve for $\mu^{*2}=1.00$ and $Q^{*2}=1.00$, where ◇ represent the densities of coexisting vapor ρ_v^* and liquid ρ_l^* phases, × represent the rectilinear diameter values, and ● represents the estimated critical point T_c^* obtained from Gibbs-ensemble Monte Carlo simulations.

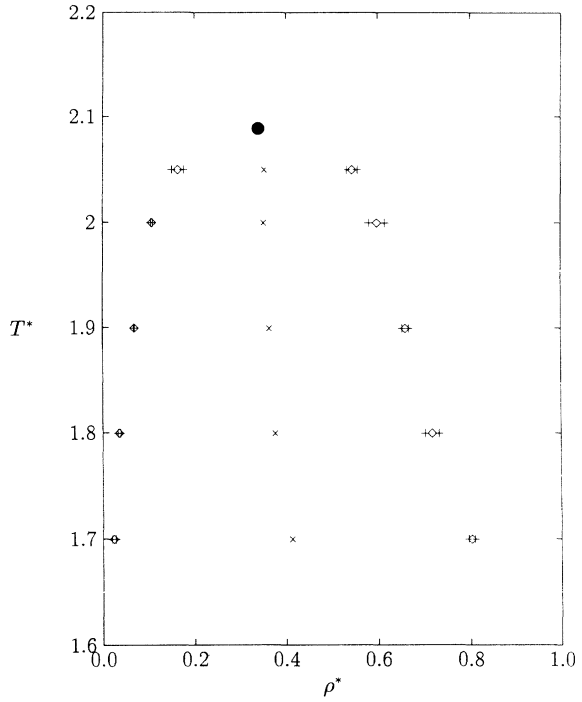

FIG. 2. Vapor-liquid coexistence curve for $\mu^{*2}=1.00$ and $Q^{*2}=1.50$. See the caption of Fig. 1 for details.

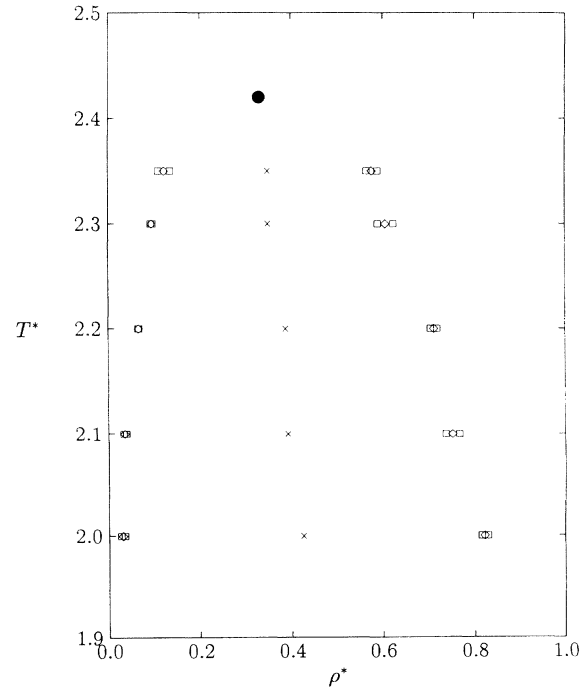

FIG. 3. Vapor-liquid coexistence curve for $\mu^{*2}=1.00$ and $Q^{*2}=2.00$. See the caption of Fig. 1 for details.

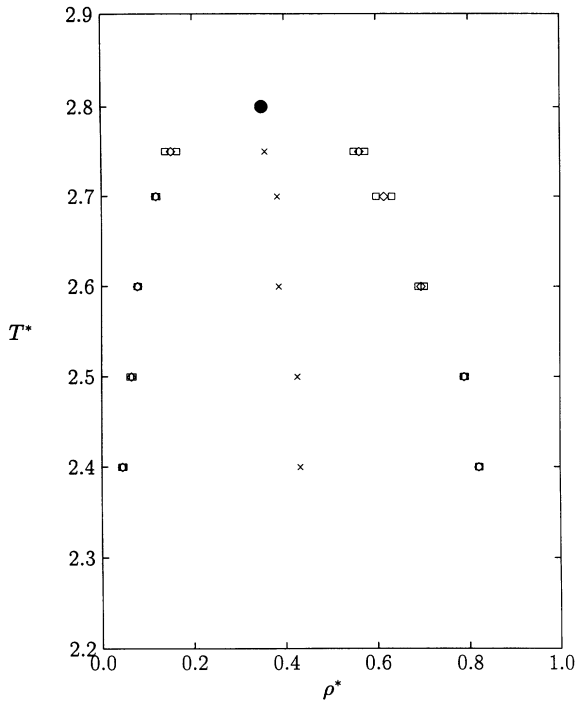

FIG. 4. Vapor-liquid coexistence curve for $\mu^{*2}=1.00$ and $Q^{*2}=2.50$. See the caption of Fig. 1 for details.

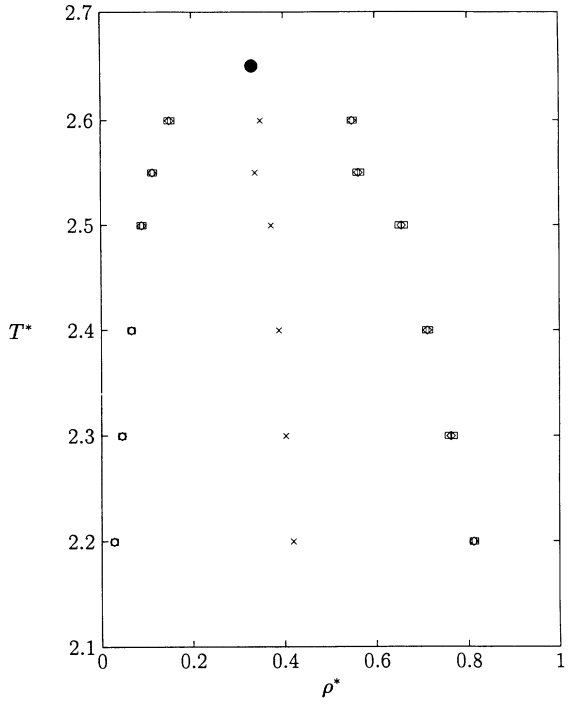

FIG. 6. Vapor-liquid coexistence curve for $\mu^{*2}=2.00$ and $Q^{*2}=2.00$. See the caption of Fig. 1 for details.

[6] and quadrupolar LJ fluids [14]. For the Stockmayer case, as μ^{*2} changes from 1.00 to 2.00, the critical temperatures move from 1.41 to 1.60, whereas the critical density hardly changes at all, moving only from 0.30 to 0.31. But for the quadrupolar LJ fluid, as Q^{*2} changes from 1.00 to 2.50, in steps of 0.50, the respective critical temperatures are 1.60, 1.89, 2.25, and 2.62, and the corresponding critical densities are 0.34, 0.36, 0.38, and 0.41. Our results for nonzero values of both moments seem qualitatively consistent with this pattern.

As a part of this investigation, we examined the behavior of the systems under the law of corresponding

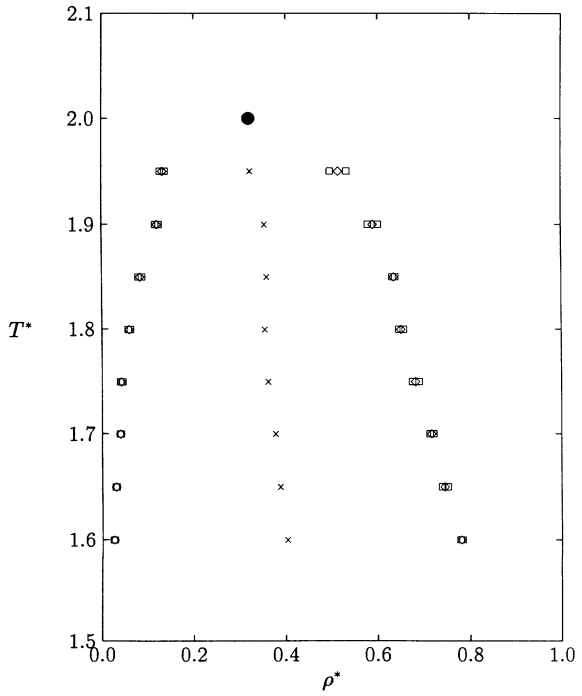

FIG. 5. Vapor-liquid coexistence curve for $\mu^{*2}=2.00$ and $Q^{*2}=1.00$. See the caption of Fig. 1 for details.

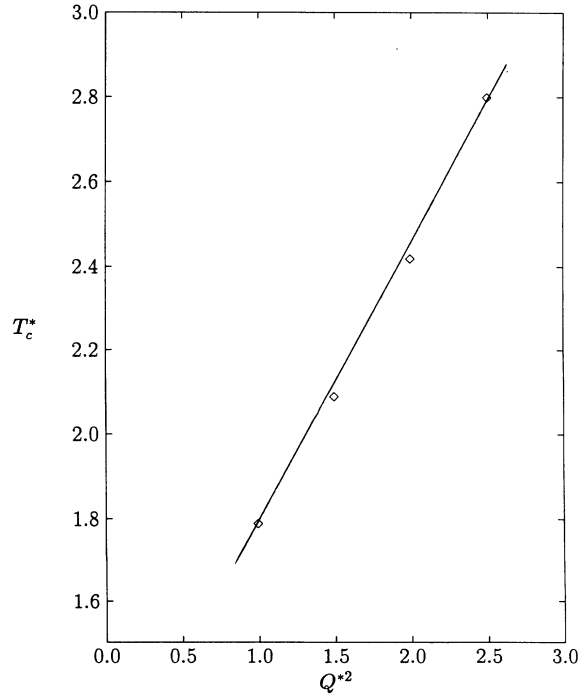

FIG. 7. Reduced critical temperature, T_c^* vs Q^{*2} for fixed $\mu^{*2}=1.00$.

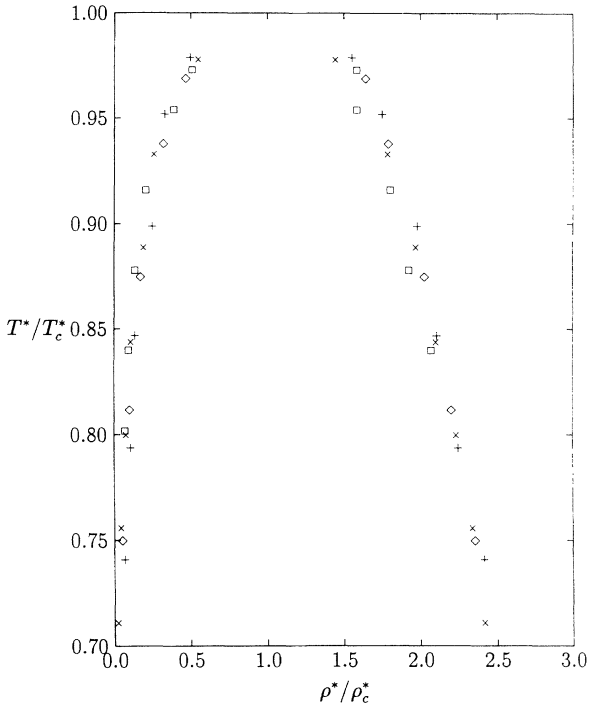

FIG. 8. The reduced vapor-liquid coexistence curves for, $\mu^{*2}=0.00$ and $Q^{*2}=1.00$, 1.50, 2.00, and 2.50, where $\Diamond$, $+$, $\Box$, and $\times$ represent for $Q^{*2}=1.00$, 1.50, 2.00, and 2.50, respectively, and $\mu^{*2}=0.00$ in all cases. The temperature and density for each system has been reduced by the respective critical temperature and density of Smit and Williams [14].

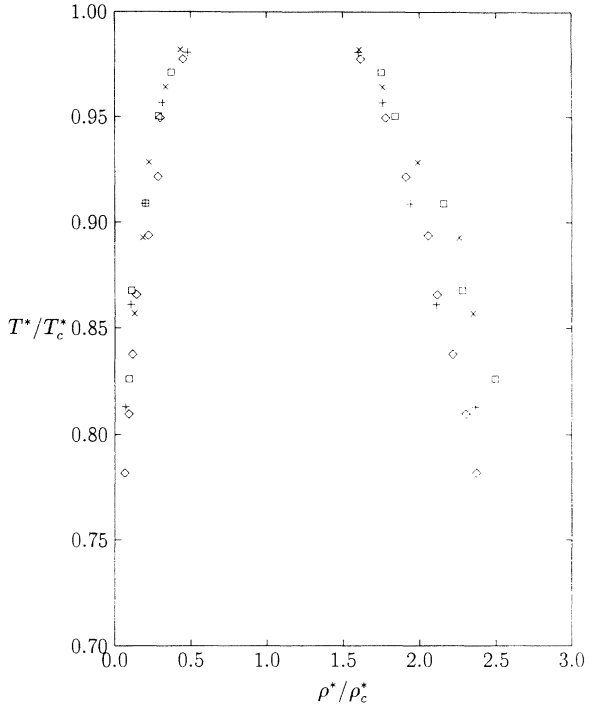

FIG. 9. The reduced vapor-liquid coexistence curves for, $\mu^{*2}=1.00$ and $Q^{*2}=1.00$, 1.50, 2.00, and 2.50, where $\Diamond$, $+$, $\Box$, and $\times$ represent for $Q^{*2}=1.00$, 1.50, 2.00, and 2.50, respectively, and $\mu^{*2}=1.00$ in all cases. The temperature and density for each system has been reduced by the respective critical temperature and density.

states. For this purpose we wanted to make a comparison between the reduced vapor-liquid coexistence curves for the quadrupolar Lennard-Jones fluid for $\mu^{*2}=0.00$, Q^{*2} not equal to 0.00 of Smit and Williams [14] and with our simulation results. As Fig. 8 shows, the law of corresponding states is largely obeyed by the quadrupolar Lennard-Jones fluid. Our results for $\mu^{*2}=1.00$ and various values of Q^{*2} (Fig. 9) show less satisfactory agreement, especially on the high density arm of the reduced coexistence curve. The scatter in the data is large, but the results suggest there is a definite effect.

For all combinations of μ^{*2} and Q^{*2}, the simulation results for the logarithm of the vapor pressure versus inverse temperature are approximately linear, as predicted by the Clausius-Clapeyron equation and by formal theories such as perturbation theory.

Patey and Valleau [24] reported the success of the Padé version of the thermodynamic perturbation theory for fluids of hard spheres with embedded point dipoles and quadrupoles. It would be very interesting to compare the results of these simulations with the predictions of thermodynamic perturbation theory.

IV. CONCLUDING REMARKS

We have presented data for vapor-liquid coexistence curves of generalized Stockmayer fluids based on Gibbs-ensemble simulations. Both T_c^* and ρ_c^* increase with increasing values of the electrostatic moments, and both are more sensitive to Q^{*2} than to μ^{*2}. We have presented results for a range of values of μ^{*2} and Q^{*2}. The behavior of T_c^* is strongly systematic with the value of the moments, but ρ_c^* is much less variable, to the point where the uncertainties are comparable with or larger than the systematic variation. Perturbation theories are known to be inaccurate for the critical parameters of the Stockmayer fluid and are likely to be even more unreliable here. However, the data presented here should prove useful when studying the systematics of liquid-vapor equilibrium in these simple model systems.

ACKNOWLEDGMENTS

This work is supported by a grant from the Natural Sciences and Engineering Research Council of Canada. Critical comments by Professor Godfrey Gumbs are greatly appreciated.

[1] W. W. Wood, in *Physics of Simple Liquids,* edited by H. N. V. Temperley, J. S. Rowlinson, and G. S. Rushbrook (North-Holland, Amsterdam 1968), Chap. 5.
[2] A. Z. Panagiotopoulos, Mol. Phys. **61**, 813 (1987).
[3] K. E. Gubbins, Mol. Simul. **2**, 223 (1989).
[4] A. Z. Panagiotopoulos and M. Stapleton, Fluid Phase Equil. **53**, 133 (1989).
[5] A. Z. Panagiotopoulos, N. Quirke, M. Stapleton, and D. J. Tildesley, Mol. Phys. **63**, 527 (1988).
[6] B. Smit, C. P. Williams, E. M. Hendriks, and S. M. de

Leeuw, Mol. Phys. **68**, 765 (1989).
[7] S. W. de Leeuw, B. Smit, and C. M. Williams, J. Chem. Phys. **93**, 2704 (1990).
[8] L. Vega, E. de Miguel, L. F. Rull, G. Jackson, and I. A. McLure, J. Chem. Phys. **96**, 2296 (1992).
[9] A. Z. Panagiotopoulos, Mol. Phys. **62**, 701 (1989).
[10] R. P. Singh, K. S. Pitzer, J. J. de Pablo, and J. M. Prausnitz, J. Chem. Phys. **92**, 5463 (1990).
[11] J. G. Amar, Mol. Phys. **67**, 739 (1989).
[12] E. N. Rudisill and P. T. Cummings, Mol. Phys. **68**, 629 (1989).
[13] M. R. Stapleton, D. J. Tildesley, A. Z. Panagiotopoulos, and N. Quirke, Mol. Simul. **2**, 147 (1989).
[14] B. Smit and C. P. Williams, J. Phys. Condens. Matter **2**, 4281 (1990).
[15] B. Smit and D. Frenkel, Mol. Phys. **74**, 35 (1991).
[16] E. de Miguel, L. F. Rull, M. K. Chalam, and K. E. Gubbins, Mol. Phys. **71**, 1223 (1990).
[17] A. Yethiraj and C. K. Hall, Mol. Phys. **72**, 619 (1991).
[18] J. J. de Pablo and J. M. Prausnitz, Fluid Phase Equil. **53**, 177 (1989).
[19] J. J. de Pablo, J. M. Prausnitz, H. J. Strauch, and P. T. Cummings, J. Chem. Phys. **93**, 7355 (1990).
[20] E. de Miguel and M. P. Allen, Mol. Phys. **76**, 1275 (1992).
[21] B. Smit, Ph.D. thesis, University of Utrecht, 1990 (unpublished).
[22] G. Stell, J. C. Rasaiah, and H. Narang, Mol. Phys. **23**, 393 (1972).
[23] G. Stell, J. C. Rasaiah, and H. Narang, Mol. Phys. **27**, 1393 (1974).
[24] G. N. Patey and J. P. Valleau, J. Chem. Phys. **64**, 170 (1976).
[25] M. P. Allen and D. J. Tildesley, *Computer Simulation of Liquids* (Clarendon, Oxford, 1987).
[26] B. Widom, J. Chem. Phys. **39**, 2808 (1963).
[27] H. Kornfeld., Z. Phys. **22**, 27 (1924).
[28] J. S. Rowlinson and F. L. Swindon, *Liquids and Liquids Mixtures,* 3rd ed. (Butterworths, London 1982).